Thermal Management of a Low-Cost 2kW Solar Inverter

LEFEVRE Guillaume, DEGRENNE Nicolas, MOLLOV Stefan

Mitsubishi Electric R&D Centre Europe - MERCE
1 allée de Beaulieu, CS 10806, 35708
Rennes, France
E-Mail: g.lefevre@fr.merce.mee.com
URL: http://www.fr.mitsubishielectric-rce.eu

Keywords

«Thermal management», «Heat-sink», « Natural convection », «Thermal vias», «Low-cost»

Abstract

This paper presents a cost-optimized thermal solution for a 2kW solar inverter. It relies on a natural convection and through-PCB thermal strategy to increase reliability and reduce cost. A methodology is described to optimize the heat-sink, as well as thermal interfaces, with the analytical approach confirmed by finite element analysis. An experimental set-up is used to validate the methodology.

Introduction

When designing a solar inverter for residential applications, the designer must define the best trade-off between several objectives including: (a) Reliability, i.e. ensuring a minimum life-time, (b) Power density, i.e. for a given power, minimizing the volume, and (c) Low-cost, i.e. minimizing components and manpower related costs. In this context, thermal management is a key point. Indeed, the thermal efficiency impacts the reliability through the device operating temperature, while significantly contributing to the overall volume – either with natural or forced convection. In fact, heat-sinks along with other apparatus such as insulating foils, fans and mechanical connections may contribute to as much as 20% of the overall converter cost.

Recent progress in power electronics has demonstrated increased efficiency beyond 98%, thus reducing the amount of losses to extract. Consequently, natural convection appears as a good candidate, more especially for systems of a few kW. Furthermore, this solution is intrinsically more reliable and less energy consuming than forced convection because it does not require fan. To remain in the aforementioned power range, only discrete components are considered in this paper, (SMD and through-hole) although the methodology could be used with power module.

The choice of a cooling system is closely related to the mechanical constraints with the power board. In terms of mechanical assembly, two solutions are widely implemented (Fig.1 and 2) depending on the devices characteristics (through-hole or SMD). In both solutions, power devices are connected to the heat-sink through an insulating foil. The solution of Fig.1, dedicated to through-hole packages like TO247, requires manpower to fold the terminals and install the mechanical clamp. In Fig.2, the components are directly soldered on the board which implies using vias or inlays to achieve the thermal transfer [3]. The former solution was rejected because the packages are not adequate to benefit from the latest generation of SiC, GaN or Superjunction devices due to parasitic inductances (~10nH/ terminals). Eventually, the second solution was preferred to be used with D²Pak components (TO263).

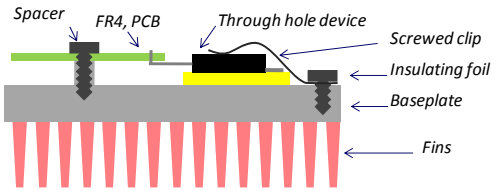

Fig. 1: Through-hole devices dedicated assembly

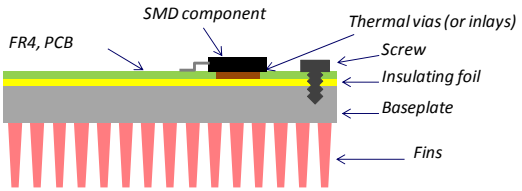

Fig. 2: SMD devices dedicated assembly

In this paper, a cost-motivated thermal design process is presented. First, the basic mechanisms of heat extraction (convection/radiation) are analytically derived to understand how the thermal resistance evolves with respect to the geometrical parameters. Then, an optimal fin arrangement is proposed to obtain the required thermal resistance, R_{th}, while reducing the cost. Afterwards, an optimization of the thermal interfaces is described where a technique to enhance thermal vias effectiveness is proposed. The methodology is validated with experimental measurements using a dedicated prototype.

Set of Specifications for the Power Converter

The electrical and mechanical specifications are summarized in Table I. The mechanical arrangement is depicted in Fig.3. Note the height of the heat-sink is imposed by the passive components (inductors and capacitors) located on the bottom side, with the goal being to build a compact system.

Table I: Basic set of specifications

Converter (Single Phase, INDOOR USE)	
Rated power	2kW
Minimum efficiency	96% (~80W losses)
Losses Distribution	
12.5% losses – 10W	5 units
4% losses – 3.2W	4 units
2% losses – 1.6W	11 units

Heat-sink	
Width	L_{base}=135mm
Length	L=235mm
Height	< 60mm w/ baseplate

Fin Temperature	Max 85°C (NF-EN60335)
Ambient Temp.	T_{amb_max} = 40°C

Under the worst operating conditions, the junction temperature T_J must remain below 125°C to maintain lifetime and reliability requirements. Consequently, the thermal gradient between junction and ambient air is $\Delta T_{J\text{-}Amb}$=85°C, distributed among the fins, spreader and insulating sheet, as well as inside the thermal connection throughout the board and the package. With the given parameters, the temperature between the fins and the quiescent air has to be lower than 45°C ($R_{th_heat\text{-}sink} \leq$0,56°C/W).

Analytical Derivation of Natural Convection and Radiation

Preamble

In spite of the apparent simplicity of convection, a stringent analytical derivation is almost impossible except for a few basic cases. Consequently, designers mostly use correlation functions stemming from dimensionless analysis and experimental measurements to define the convection coefficient *h* [4].

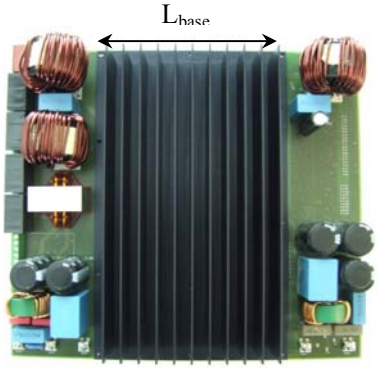

Fig. 3: Picture of the prototype

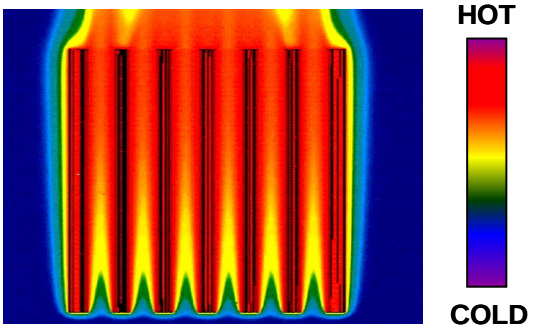

Fig. 4: Thermal boundaries over a heated heat-sink

The heat-sink can be reasonably described as a combination of channels [5][6] instead of using plane plates correlation [4]. Indeed, in the case of a plate, both mechanical and thermal boundary layers can freely expand (developing flow), taking advantage from fresh air outside the boundary layers. In the case of heat-sink, the boundary layers may join (fully developed flow) as depicted in Fig.4 which increases the fluid temperature in between and degrades the heat extraction. Note in Fig.4 the different thermal behaviour between inner and outer fins. Eventually, one can understand that the inter-fin spacing is an optimisation variable. Small values mean larger area with degraded *h* whereas widely spaced fins improve *h* at the cost of a reduced area.

Table II summarizes the dimensionless variables used in this analysis. The fluid properties should be evaluated at the film temperature, which is the mean temperature between quiescent fluid and surface.

Table II: Dimensionless numbers and definitions of variables

Number	Physical meaning	Expression
Prandtl Pr	Viscosity/ Thermal diffusivity	$\mathrm{Pr} = \frac{\mu \cdot c_P}{\lambda}$
Nusselt Nu_L	Conduction/ Convection	$Nu_L = \frac{h \cdot L}{\lambda}$
Grashoff Gr_L	Buoyancy/ Viscosity	$Gr_L = \frac{g \cdot \beta \cdot \Delta T \cdot L^3}{\nu^2}$
Rayleigh Ra_L	Momentum/ Thermal diffusivity	$Ra_L = Gr_L \cdot \mathrm{Pr}$

ΔT : temperature between fluid and surface (K)
g : Acceleration (9.81 $m \cdot s^{-2}$)
β : Thermal expansion coefficient ($\approx 1/T$ for gas)
ν : Kinematic viscosity ($m^2 \cdot s^{-1}$)
c_p : Specific heat ($J \cdot kg^{-1} \cdot K^{-1}$)
h : Convection coefficient ($W \cdot m^{-2} \cdot K^{-1}$)
λ : Thermal conductivity ($W \cdot m^{-1} \cdot K^{-1}$)
μ : dynamic viscosity ($kg \cdot m^{-1} \cdot s^{-1}$)
L : characteristic length (m)

Analytical model of a heat-sink under natural convection

In this section, an accurate model is investigated to define the average convection coefficient for a given geometry. First, a basic geometry is defined in Fig.5. To avoid complicating the analysis, the fins are assumed to be rectangular with an adiabatic edge. Other boundary conditions and geometries can be analyzed by selecting proper fin efficiency [4]. However, the purpose of this work is to provide an easy tool rather than describing complex geometries such as corrugated or interrupted fins.

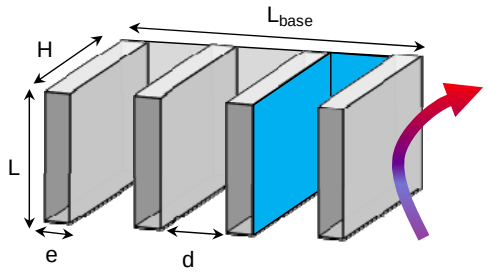

Fig. 5: Selected geometry to define convective and radiative effects in a heat-sink

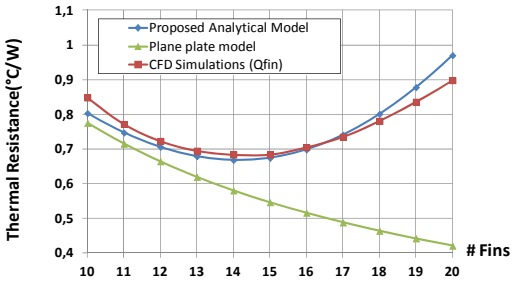

Fig. 6: Comparison between simulation and models regarding the number of fins

According to results of [7], the correlation from [6] is used to estimate the average Nusselt number of a channel (1). The Nusselt number is similar for outer fins, even if not impacted by inter-fin distances.

$$Nu_{D_H} = \left(\frac{576}{\left(Ra_{D_H} \cdot \frac{D_H}{L} \right)^2} + \frac{2.873}{\left(Ra_{D_H} \cdot \frac{D_H}{L} \right)^{0.5}} \right)^{-0.5} \quad with \quad \begin{cases} Ra_{D_H} = \frac{g \cdot \beta \cdot \Delta T \cdot {D_H}^3 \cdot \mathrm{Pr}}{\nu^2} \\ D_H = \frac{2 \cdot H \cdot d}{2 \cdot H + d} \end{cases} \tag{1}$$

Taking into account a non uniform thermal distribution, the fin efficiency (2) is calculated assuming that the thickness e is much lower than L. Note that the fin efficiency is the flux ratio between an isothermal and a fin with a finite thermal conductivity. L_c is the characteristic length of the fin (m).

$$\eta_{fin} = \frac{\tanh(H / L_c)}{H / L_c} \quad with \quad L_c \approx \sqrt{\frac{\lambda_{fin} \cdot e}{2 \cdot h}} \quad and \quad h = \frac{\lambda \cdot Nu_{D_H}}{D_H} \tag{2}$$

As mentioned in the preamble, the fin number N_{fin} is a critical design parameter. The thermal resistance is thus parameterized with respect to N_{fin} via all the geometrical variables. Given S_1, the fin area, S_2, the baseplate area without any fins, one can figure out the convective thermal resistance (3):

$$\Re_{conv}(N_{fin}) = \frac{1}{h(N_{fin}) \cdot \left(N_{fin} \cdot S_1 \cdot \eta_{fin}(N_{fin}) + S_2(N_{fin}) \right)} \tag{3}$$

In order to demonstrate the relevancy of the proposed model, CFD simulations under Qfin® have been carried out. A baseplate of 135mm width and 235mm length equipped with 40mm height fins was selected. The fin thickness was 2mm, perfectly suitable value for industrial feasibility. The baseplate and quiescent air temperatures are respectively 85°C and 40°C. Furthermore, radiation is neglected. As shown in Fig.6, the analytical model matches well with simulation whatever the thermo-mechanical flow properties (less than 10% error). It can be also be noted that the plate model is only valid when fins are not closely packed which is absolutely not suitable in our case.

Analytical model of radiative heat transfer from a heat-sink

With naturally cooled systems, radiation may contribute up to 45% to the overall heat transfer [8]. However, it is only possible to take advantage from radiation if the solar inverter is protected from other radiation sources that might contribute to the heat (as the sun for example). The intention is to get a simple and easy model for radiation instead of a complex derivation of form factors between radiating surfaces. That is why the fin efficiency is assumed high enough to neglect the impact of thermal distribution on radiation heat transfer. Validated through experimental measurements from [9], the model proposed in [10] was eventually chosen. The form factor of the blue channel depicted in Fig.5 and the total radiation flux according to Stefan-Boltzmann law are thus (4) and (5).

$$F = 1 - \frac{2 \cdot \overline{H} \cdot \left(\sqrt{1 + \overline{L}^2} - 1 \right)}{2 \cdot \overline{H} \cdot \overline{L} + \sqrt{1 + \overline{L}^2} - 1} \quad with \begin{cases} \overline{H} = H / d \\ \overline{L} = L / d \end{cases} \tag{4}$$

$$\varphi_{Rad}\left(N_{fin}\right) = \sigma \cdot \left(T^4 - T_{amb}^4\right) \cdot \left(\varepsilon \cdot S_{rad\_ext} + \left(N_{fin} - 1\right) \cdot \frac{\left(d + 2 \cdot H\right) \cdot L}{\left(1 - \varepsilon\right) / \varepsilon + 1 / F} \right) \; with \; S_{rad\_ext} = N_{fin} \cdot \left(L \cdot e + 2 \cdot H \cdot e\right) \tag{5}$$

σ : Stefan-Boltzmann's constant ($5{,}67 \cdot 10^{8}$ $W \cdot m^{-2} \cdot K^{-4}$)
ε : Emissivity. ε=0,05 for Raw Aluminium; ε=0,85 In case black painting or anodization process [8]

Design procedure for an optimised extruded profile

Methodology

A recent cost analysis among different manufacturers [11] has indicated that the cost of a heat-sink mainly depends on the mass of extruded aluminium, irrespective of the profile - in average, 8.2€ per kg of raw material is a reasonable value. Consequently reducing the overall mass comes along with a cost reduction. Several quotations confirmed that 4€/m² is roughly the cost of a specific finish. These costs assume industrial volume (typically with a MOQ of 10kunits). Basically, the previous models have been implemented in a MathCad routine to define the thermal performances with respect to the geometrical variables (height, thickness and pitch). Since the convection coefficient remains low in natural convection (<5 $W \cdot m^{-2} \cdot K^{-1}$), a reduction of the fin thickness seems possible because of quasi unitary fin efficiency. However, all manufacturers confirmed that 2mm is a minimum value to avoid altering mechanical robustness (during a sawing for instance) or requiring extra-cost with conventional extrusion. This value was thus selected to remain compliant with basic industrial processes.

Results

Based on the convection/radiation model, an optimization was carried out with and without radiation to evaluate the relevancy of special treatments (R_{th} =0,56°C/W). The results are summarized in Table III. Far more than reducing cost (nearly 10%), the power density (61 vs. 47W/L) as well as the weight (123W/kg vs. 92W/kg) are significantly improved due to the radiation.

Table III: Optimisation results (baseplate not included)

Finish	Fin number	Heigh	Mass	$Cost_{Al}$	$Cost_{Finish}$	Total Cost	Volume
NONE	13	55mm	862 g	7,1€	NONE	7,1€	1,7 L
BLACK	13	42mm	648 g	5,3€	1,3€	6,6€	1,3 L

Thermal Path Improvement between the Die and the Baseplate

Introduction

So far, the efforts have focused on the heat-sink design, independent from the thermal interfaces. Nevertheless, this point must be investigated to target a balanced design. This section is a step further to properly define the baseplate width, as well as the thermal paths (inlays or vias). Furthermore, attention will be paid to cope with the poor thermal performances of insulating foils.

To better understand the challenges, basic calculations of thermal resistances are given in the Table IV for D²Pak packages, equipped with different electrical insulating sheets withstanding at least 4kV. A thermal area S_{die} of 10mmx11mm which corresponds to a radius of 6mm is assumed. As demonstrated in [12], an adequate via pattern for D²Pak leads to a thermal resistance around 0.4°C/W per mm of PCB. On the other hand, a copper inlay of 6mm is 0.25€ with a negligible R_{th} (less than 0,1°C/W). In [13], an asymptotic value of the spreader resistance is available (6). Obviously, the final value might be higher to limit the mass of aluminium but the order of magnitude remains in the same range.

$$\Re_{baseplate} = \frac{\pi}{4\cdot\sqrt{2}} \cdot \frac{1}{\lambda_{baseplate}\cdot\sqrt{S_{die}}} \approx 0{,}3°C/W \text{ with } \lambda_{baseplate} = 171\ W/m\cdot K \text{ and } S_{die} = 10mm\times 11mm \qquad (6)$$

Table IV: Distribution of thermal resistances for typical insulating sheets (2mm thick PCB)

λ_{foil} ($W.m^{-1}.K^{-1}$)	$Thick_{foil}$	Rth foil (1D)	Rth vias/inlay	Rth baseplate	% foil
5.5	200µm	0.33°C/W	0.8/0.1°C/W	0.3°C/W	23/45%
1.4	250µm	1.6°C/W	0.8/0.1°C/W	0.3°C/W	60/80%
1.6	500µm	2.8°C/W	0.8/0.1°C/W	0.3°C/W	72/90%

Considering Table IV, it is apparent that the insulating sheet's contribution to the overall thermal resistance is high. In the current case, a thickness of 500µm is necessary to cope with mechanical tolerances, i.e. to fill the remaining micro-gaps located between the board and the base plate. A way to cost efficiently improve the conductive heat flux throughout the insulating sheet is thus going to be detailed. This technique can only be implemented with vias and is not suitable for copper inlays.

Analytical model of the interface between the vias and the insulating foil

Apart from improving the thermal conductivity, which usually comes along with a higher cost, only the flux area can be optimized. To reach this goal, spreaders are implemented on the bottom layer of each via pattern, acting like annular rings (Fig. 7). It has to be noted that the radius R_{int} is calculated to get the same die area as the original square die. Several FEA simulations (FEMM 4.2) confirmed that the bottom side of the insulating sheet is isothermal if the baseplate is thick enough (thermal bypass).

The vias pattern cannot be accurately modelled because of a 3D geometry and it is assumed the die is directly located on the bottom layer. Obviously, the results stemming from this approach only give the minimum thermal resistance that can be achieved since in the real case, the flux is not able to freely spread and fully benefit from the spreaders. A simplified case study is detailed in Fig.8. A full derivation with Bessel functions could have been possible but the physical insight is less intuitive [14].

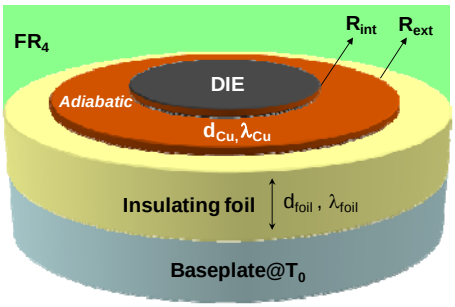

Fig. 7: Reference geometry

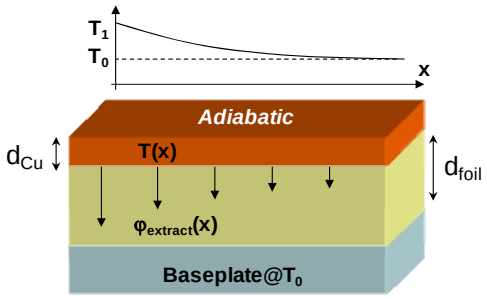

Fig. 8: Simplified 1D geometry

Based on the Fig. 8, the heat flux (per area) from the fin to the baseplate is (7). Note this implies the flux in the foil is 1D which is not valid when the fin is no longer isothermal. An equivalent convection coefficient can be defined to use (2) as well as a length L_c to more clearly define the validity range (8)

$$\varphi_{extract}(x) = \lambda_{foil} \cdot \frac{\partial T(x)_{z=0}}{\partial z} \approx \frac{\lambda_{foil}}{d_{foil}} \cdot (T(x) - T_0) \quad \rightarrow \quad h_{eq} = \frac{\lambda_{foil}}{d_{foil}} \tag{7}$$

$$L_c \approx \sqrt{\frac{\lambda_{Cu} \cdot d_{Cu}}{h_{eq}}} = \sqrt{\frac{\lambda_{Cu}}{\lambda_{foil}} \cdot d_{Cu} \cdot d_{foil}} \tag{8}$$

To easily take into account the radial geometry, correction functions are available in [14]. The Schmidt approach (9) was selected among all because of the best trade-off between accuracy and complexity. The fin efficiency of an annular ring (Fig.7) with internal and external radia R_{int}, R_{ext} is given by (10).

$$F_{Corr} = 1 + 0{,}35 \cdot \ln(R_{ext} / R_{int}) \tag{9}$$

$$\eta_{Ann.Fin} = \frac{\tanh((R_{ext} - R_{int}) \cdot F_{Corr} / L_c)}{(R_{ext} - R_{int}) \cdot F_{Corr} / L_c} \tag{10}$$

Due to the definition of fin efficiency (performance ratio with an isothermal fin), an equivalent external radius of an isothermal fin can be used, as per (11).

$$R_{Eq} = \sqrt{(R_{ext}^2 - R_{int}^2) \cdot \eta_{Ann.Fin} + R_{int}^2} - R_{int}^2 \tag{11}$$

Since the fin is now modelled as an equivalent isothermal annular ring, it is possible to estimate the thermal resistance across the insulating sheet, including spreading effect (2D approach). A fair comparison of models [13][15][16] and simulations carried out under FEMM4.2 have shown that a spreading angle of 45° can be used with good accuracy (12). The model from [15] is based on an analytical solving of thermal differential equations assuming an isothermal boundary on the bottom layer. In spite of an affordable complexity, Bessel functions are necessary, which is not the target.

$$\Re_{Th\ w/\ spreader}(\varphi) = \frac{d_{iso}}{\lambda_{iso}} \cdot \frac{1}{\pi \cdot (R_{int} + R_{Eq})^2 \cdot (1 + d_{iso} \cdot \tan\varphi / (R_{int} + R_{Eq}))} \tag{12}$$

As an example, a die with R_{int} =5mm mounted with a 500µm thick sheet and λ_{foil}=1,5W·m^{-1}·K^{-1} has been studied. In Fig.8 to Fig.10, results are given for d_{cu}=35µm, 70µm and 105µm. The specific case of an ideal isothermal fin has been computed to define the best trade-off and avoid increasing needlessly the spreader. Additional simulations confirmed consistent results for higher thermal conductivities and different inner radii as well. In the current example, one can understand that 2 to 3 mm is a good technical compromise, the fin efficiency plummeting for higher diameters.

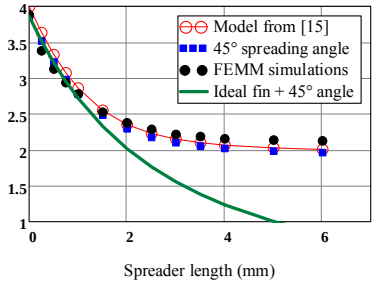

Fig. 9: R_{th} (°C/W) for d_{Cu}=35µm and R_{int} =5mm (D²Pak)

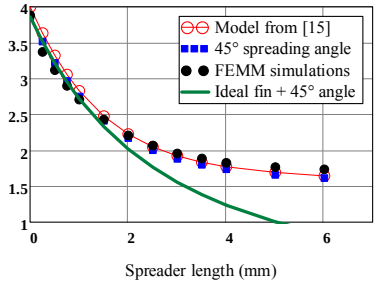

Fig. 10: R_{th} (°C/W) for d_{Cu}=70µm and R_{int} =5mm (D²Pak)

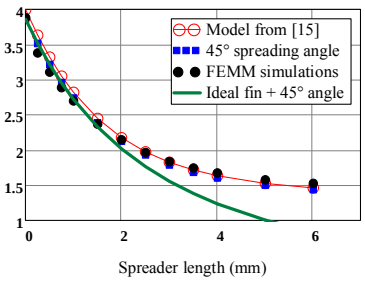

Fig. 11: R_{th} (°C/W) for d_{Cu}=105µm and R_{int} =5mm (D²Pak)

In practice, the real thermal resistance is lower than the value without any spreader (around 4°C/W in the aforementioned example) but higher than the asymptotic value from the model. To further tend to the asymptotic value, balancing layers are implemented in the vias pattern to emulate a spreading effect layer by layer as depicted in Fig.12. Because of a high complexity, the relevancy of this mechanical arrangement is demonstrated with experimental measurements in the following section.

Experimental validation for thermal path between the die and the baseplate

To validate the model, a PCB with different spreaders was designed as depicted in Fig.13 (top and bottom views). One of the test cases specifically includes a copper plane on each layer (Fig.12) to balance the thermal constraints over the vias paths and ensures a more uniform heat flux on the bottom side as a massive spreader would permit. A copper thickness of 70µm was selected for all layers of the experimental board. The via pattern, composed by 110 holes (drilling diameter of 0.35mm, 25µm barrel thickness) has not been designed in a sake of optimization. According to [12], the thermal resistance can be realistically reduced from 1.4°C/W to 0.9°C/W by doubling the number of holes.

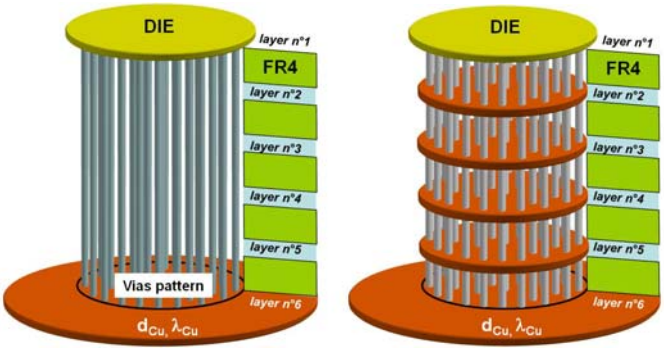

Fig. 12: Vias pattern with and without balancing plates

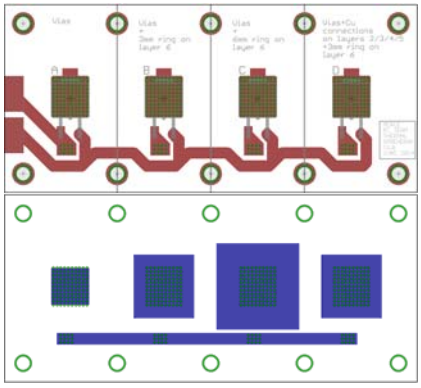

Fig 13: Experimental validation board

Details about the sample tests are given in Table V. Each pattern is equipped with a D²Pak resistance supplied to generate 10W and 20W. The board is screwed on a heat-sink (forced convection), and equipped with thermocouples. First, measurements were carried out with a D²Pak die attached to a massive block of aluminium to avoid an inhomogeneous thermal distribution from the die to the vias. No differences were observed when the die is directly mounted on the board or on a copper spreader.

Table V: Mechanical arrangements available on the experimental platform

Case	A (Reference)	B	C	D
Spreader (mm) (Fig.13)	no	3mm	6mm	3mm
Balancing plate (Fig.12)	no	no	no	yes

The Fig. 14 summarizes the comparative results of tests. Additionally, the overall thermal resistance (between the bottom side of the die to the heat-sink) is depicted in Fig.15 as well as an estimated value for inlays (6mm radius). It can be noted that the balancing layers help reduce the thermal resistance (Case D) and a too wide spreader is unnecessary as expected by the fin efficiency theory (Case C). The comparison in Fig.15 shows the performances of inlays (estimated 2,6°C/W with a 45° spreading angle) cannot be outperformed with the current geometry but an equivalence can be nearly obtained by optimizing the vias due to a reduction of 0.5°C/W as mentioned previously. In such a case, this solution would take the edge over copper inlays because of cost-effectiveness.

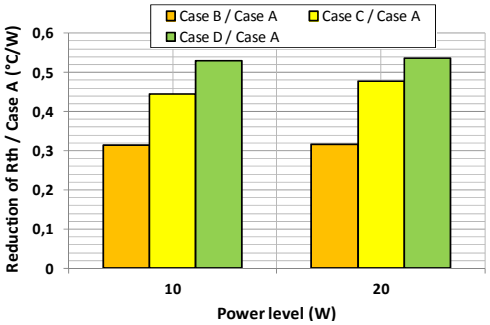

Fig. 14: Comparative results obtained from experimental measurements

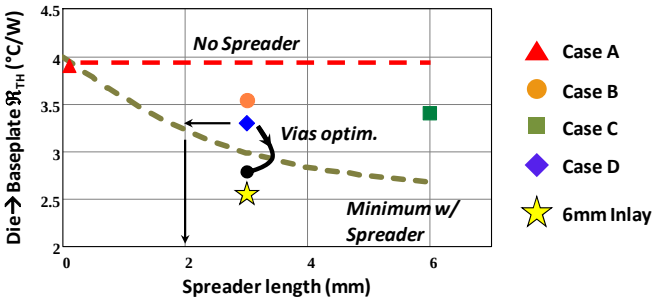

Fig. 15: Overall comparison (experimental)

Choice of an Adequate Baseplate Thickness

The baseplate thickness is a critical point to spread the flux on top of the fins. While the fins number and the pitch define the average temperature over the bottom side of the baseplate, the spreading effect is responsible for hot spots. A thin baseplate refrains the thermal flux from equitably diffusing, thus leading to a high spreading resistance. On the other hand, an excessive thickness fixes this issue at the cost of higher volume and price. This theme has been widely investigated over years [13][15], historically by Kennedy in the early 60's [17]. Most of them consist of transforming a rectangular into a cylindrical geometry with similar area (die and baseplate) to alleviate mathematical constraints and permit an analytical solution. The heat-sink is then replaced by an equivalent h_{eq} coefficient (Fig.14).

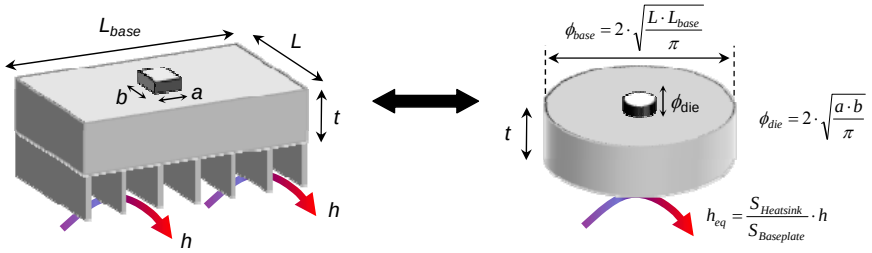

Fig. 16: Geometrical equivalence to estimate the spreading resistance inside the baseplate

The results from [13] were compared to FEMM4.2 simulations with the baseplate modelled as a disk of radius $(235 \cdot 135)^{0.5}/\pi \approx 100$mm. Assuming a convective $\Re_{th}$ of 0,56°C/W, the equivalent coefficient h_{eq} is 55 $W \cdot m^{-2} \cdot K^{-1}$, Fig.17 summarizes the results with the motivation being to spread the flux in other layers, different equivalent dies radii were chosen to anticipate the impact of annular rings located just on top of the baseplate : 5mm and 8mm. Using (6), the asymptotic values of spreading resistances are respectively 0,36°C/W and 0.23°C/W. In spite of underestimating by nearly 15%, this formula is a good rule of thumb to understand how the overall thermal resistance is distributed.

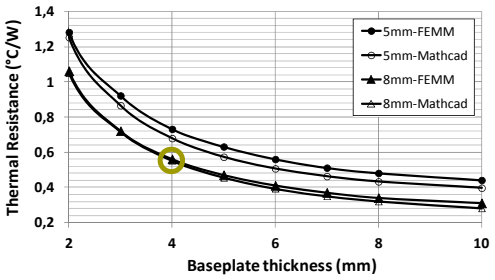

Fig. 17: Comparison simulation-model for various die radii and baseplate thicknesses

Fig. 18: Picture of the designed heat-sink

In the final prototype, the vias have been designed according to case D as presented in the previous section. According to experimental measurements of Fig.15, the 3mm spreader and balancing plates reduce the thermal resistance of the insulating layer to nearly 3.3°C/W. Using the same figure, the equivalent die diameter to consider is 8mm (6mm + 2mm of equivalent additional spreader).

It is thus possible to use results from Fig.15 (8mm) to define the proper thickness to reduce cost without degrading the technical performances. As previously mentioned, the PCB board is directly mounted on the baseplate with M3 screws (3mm). As a rule of thumb, the drilled depth must be at least $2 \cdot \phi_{screw}$ for soft metals like Aluminium. Since the power board is around 2mm thick, this implies a minimum thickness of 4mm with an expected baseplate thermal resistance of 0,5°C/W.

Experimental Results of the Overall Thermal Solution

To avoid a custom extrusion, a sub-optimal design based on Cooltec CT191® was preferred (Fig.18). The baseplate thickness was reduced from 5mm to 4mm. After taking off two fins to obtain an external frame, the heat-sink is composed by 11 fins of 45mm height and 2.25mm thick. Performances are similar to the optimized design, higher height partially counterbalancing two missing fins. Thus,

the overall cost is calculated to be around 11€ distributed between fins (710g ⇔ 5.8€), baseplate (350g ⇔ 2.9€) and surface finish (0,35m² ⇔ 1,4€), with an additional euro for the tool cost.

With the thermal validation tests, a bare board was mounted with 16 D²Pak resistances to emulate the 80W dissipated by the active components (MOS and diodes). The values were chosen to generate either 10W or 3.2W or 1.6W. Finally, a 500µm thick insulating sheet with a thermal conductivity of 1,5 $W.m^{-1}.K^{-1}$ (t-Global Technology, Series L37-5) interfaces the board with the heat-sink. Four points located at 5cm from every corner of the bottom side (fins), as well as one in the middle, have been used to estimate the average temperature over the baseplate. Regarding the validation of the annular ring concept with the experimental prototype, an IR cam (Flir i50) together with thermocouples was selected. The accuracy of Flir i50 is $\pm 2\% \cdot T_{meas} \pm 2°C$.

First, measurements were carried out to compare the analytical model of fins under natural convection/radiation. In addition, the model of a raw aluminium heat-sink is displayed in Fig.19 to justify the relevancy of anodizing the device. During the tests, the ambient temperature was around 26°C. The accuracy range is displayed with gray markers. The results are consistent with those predicted by calculation and clearly highlight the importance of radiation in the overall heat extraction (+15%). The Fig.20 represents a thermography of the bottom baseplate. The temperature is homogeneous with extreme values 10% deviated from the average value. In spite of a small baseplate thickness, the distributed losses distribution naturally spreads the flux, getting rid of local hot spots. Assuming an ambient temperature of 40°C, requirements are thus met (less than 85°C) so much the more that convection and radiation are more effective at higher temperatures.

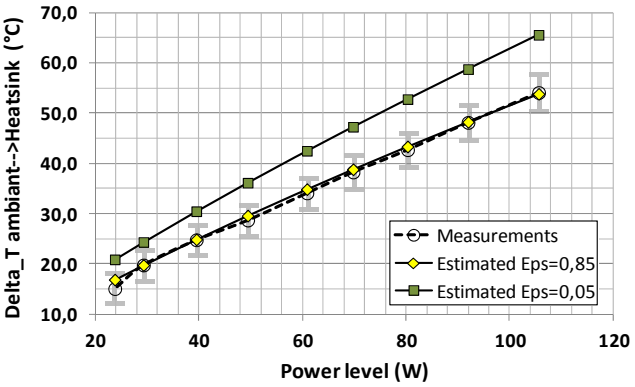

Fig. 19: Comparison between analytical model and measurements for the designed heat-sink

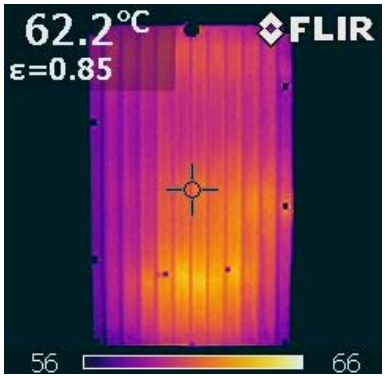

Fig. 20: Thermography of the heat-sink bottom side dissipating 80W

Secondly, the temperature over the most constrained die was measured to validate the thermal resistance of interfaces. From calculations, a thermal resistance of 3.8°C/W is expected. The thermal distribution over the baseplate and the die metallization are given in Fig.21 and Fig. 22. A linear approximation of the thermal gradient with respect to the dissipated power led to 4°C/W, value close to the calculation. With this set of parameters, a maximum junction temperature of 125°C will not be exceeded, assuming a junction to case thermal resistance of 0.5°C/W (typical value for D²Pak).

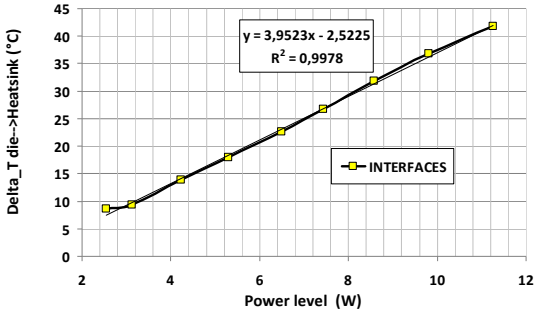

Fig. 21: Measurements of the die temperature for various power levels

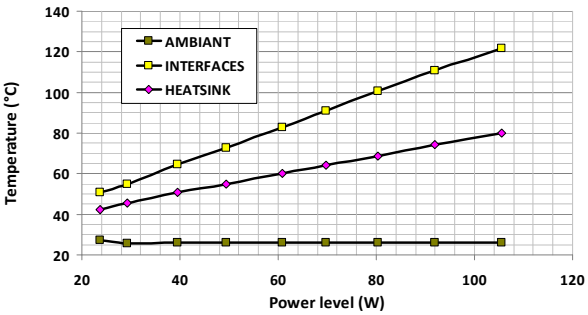

Fig. 22: Measurements of temperatures over the heat-sink and the bottom side of the die

Conclusions

In this paper, a design methodology was presented to improve the cost of the thermal solution for a 2kW converter. In order to limit manpower efforts necessary with through- hole transistors and diodes, a direct cooling technique using SMD components and thermal vias was promoted. The design of both heat-sink and thermal interfaces was thus investigated. Using an analytical approach, the geometrical properties (fin height and inter-fin spacing) of a naturally cooled heat-sink have been defined, with the goal being to reduce the extruded mass as much as possible. Experimental measurements validated the results of this optimization process. Then, the impact of the insulating sheet was highlighted and a way to spread the flux with additional copper rings was presented. To cope with the thermal anisotropy of vias which affect the effectiveness of this solution, balancing copper planes have been added on every internal layer to act as a local spreader. Results obtained with different geometries demonstrated the spreader with balancing planes and with an optimized vias pattern could be as efficient as copper inlays. Thus, with the proposed methodology, the overall cost is around 15€, including the heat-sink, the insulating sheet and the extra operations for PCB.

References

[1] S. V. Araujo, P. Zacharias, and R. Mallwitz, “Highly efficient single-phase transformerless inverters for grid-connected photovoltaic systems” IEEE Trans. Ind. Electron., vol. 57, no. 9, pp. 3118–3128, Sep. 2010

[2] Bin Gu; Dominic, J.; Jih-Sheng Lai; Chien-Liang Chen; LaBella, T.; Baifeng Chen, "High Reliability and Efficiency Single-Phase Transformerless Inverter for Grid-Connected Photovoltaic Systems," Power Electronics, IEEE Transactions on , vol.28, no.5, pp.2235,2245, May 2013

[3] Marz, M., "Thermal management in high-density power converters" Industrial Technology, 2003 IEEE International Conference on, vol.2, no., pp.1196,1201 Vol.2, 10-12 Dec. 2003

[4] R. Remsburg, "Thermal design of Electronic equipment", CRC Handbook, 2001

[5] W. Elenbaas, "Heat Dissipation of Parallel Plates by Free Convection," Physica, Vol. IX, No. 1, pp. 1 – 28,1942

[6] A. Bar-Cohen, and W. M. Rohsenow, "Thermally Optimum Spacing of Vertical, Natural Convection Cooled, Parallel Plates", ASME Journal of Heat Transfer, Vol. 106, pp. 116-123, 1984

[7] Golnoosh M. , « Natural Convective Heat Transfer from Interrupted Rectangular Fins”, Thesis submitted in partial fulfilment of the requirements for the degree of Master of Applied Science, Simon Fraser University , 2012

[8] Aavid Thermalloy “Effect of anaodization on radiationnal heat transfer”
Internet : http://www.aavid.com/product-group/extrusions-na/anodize

[9] Rea, S. and West, S., “Thermal Radiation from Finned Heat-sinks,” IEEE Transactions on Parts, Hybrids and Packaging, Vol. PHP-12, No. 2, June 1976, pp. 115 – 117

[10] Shabany, Y., “Radiation Heat Transfer from Plate-Fin Heat-sinks,” Proceedings of 24th Annual IEEE Semiconductor Thermal Measurement and Management Symposium (SemiTherm 24), March 16 - 20, 2008, San Jose, CA, Pages 133 - 137

[11] Lefevre, G.; Rambaud, L.; Foube, L.; Mollov, S., "Low-cost designs for domestic photovoltaic applications," Power Electronics and Applications (EPE), 2013 15th European Conference on, 2-6 Sept. 2013

[12] Gautam, D.; Wager, D.; Musavi, F.; Edington, M.; Eberle, W.; Dunford, W.G., "A review of thermal management in power converters with thermal vias," Applied Power Electronics Conference and Exposition (APEC), 2013 Twenty-Eighth Annual IEEE, pp.627,632, 17-21 March 2013

[13] S. Song, S. Lee, and V. Au, “Closed-form equation for thermal constriction/spreading resistances with variable resistance boundary condition,” Proc. 1994 IEPS Tech. Conf., pp. 111–121, 1994

[14] A. Acosta-Iborra, A. Campo, “Approximate analytic temperature distribution and efficiency for annular fins of uniform thickness”, International Journal of Thermal Sciences, Volume 48, Issue 4, April 2009, Pages 773-780

[15] Yovanovich, M. M., Culham, J. R., and Teertstra, P. M., “Analytical Modeling of Spreading Resistance in Flux Tubes, Half Spaces and Compound Disks,” IEEE Transactions on Components, Packaging, and Manufacturing Technology-Part A, Vol. 21, No. 1, 1998,pp. 168–176

[16] Koito, Y, Okamoto, S. and Tomimura, T. (2014) Two-Dimensional Numerical Investigation on Applicability of 45° Heat Spreading Angle. Journal of Electronics Cooling and Thermal Control, 4, 1-11

[17] D. P. Kennedy, Spreading Resistance in Cylindrical Semiconductor Devices, Journal of Applied Physics, Vol. 31, 1960, pp. 1490-1497